Research Article

Sijia Li, Chun Shao, Zhikun Miao, and Panfang Lu*

Development of leftover rice/gelatin interpenetrating polymer network films for food packaging

https://doi.org/10.1515/gps-2021-0004
received September 10, 2020; accepted November 08, 2020

Abstract: Waste biomass can be used as a raw material for food packaging. Different concentrations of gelatin (GEL) were introduced into the leftover rice (LR) system to form an interpenetrating polymer network (IPN) for improving the properties of the films. The structure and morphology of films were evaluated by Fourier transform infrared, scanning electron microscopy, and atomic force microscopy, which showed good compatibility between LR and GEL. The moisture content and oil absorption rate of IPN films were down by 105% and 182%, respectively, which showed better water and oil resistance than the LR film. In addition, increasing GEL concentration led to enhancement in the tensile strength of films from 2.42 to 11.40 MPa. The water contact angle value of the IPN films (117.53°) increased by 147% than the LR film (47.56°). The low haze of IPN films was obtained with the increment of the mutual entanglement of LR and GEL. The 30–50% GEL addition improved the water vapor barrier and thermal stability properties of the IPN films. This study highlights that LR as waste biomass can have a practical application in food packaging.

Keywords: biocomposite, leftover rice, barrier properties, waste biomass, IPN

1 Introduction

Interpenetrating polymer network (IPN) has a special aggregate structure formed by the mutual transformation and entanglement of two or more polymers [1]. The property and structure of IPN were tailored by interpenetrating network technology [2]. Its unique entanglement structure can improve the compatibility among polymer chains, increase network density, and bonding force [3]. Kamboj et al. used the Maillard reaction between corn fiber gum and chitosan to prepare the IPN films resistant to water, acids, and alkali [4]. Jindal et al. fabricated IPN films with high crosslink density using bael fruit gum and chitosan, thereby improving the properties of GEL films [5]. As a new type of heterogeneous polymer, because of their unique chemical blending methods and network interpenetrating structure, the IPNs have been widely studied in conductive materials [6], controlled-release materials [7], damping materials [8], medical polymer functional materials [9], etc. Therefore, if the IPN structure is applied to food packaging, it will play an increasingly important role in food packaging.

Packaging facilitates the transportation of goods during production and circulation while preventing the goods from contacting pollutants [10]. The main materials of the traditional food packaging were polyethylene, polyvinyl chloride, poly(vinylidene chloride), and so on, which resulted in serious ecological and health problems [11]. At the same time, the increasing consumption of fossil fuels affects its price and sustainability [12]. These adverse effects can be mitigated by applying safe and degradable materials for food packaging films [13,14].

According to Food and Agriculture Organization of the United Nations reports, around 1.3 billion tons of food is wasted globally every year [15]. It is necessary to convert it into value-added products increasing global sustainability. Kitchen waste, as a kind of waste food source, is a relatively available high-quality feedstock. It was generally dealt with by landfilling, composting,

* **Corresponding author: Panfang Lu,** Food Safety Analysis and Test Engineering Technology Research Center of Shandong Province, College of Chemistry and Material Science, Shandong Agricultural University, Tai'an, Shandong 271018, People's Republic of China, e-mail: xiaolu980216@163.com
Sijia Li, Chun Shao, Zhikun Miao: Food Safety Analysis and Test Engineering Technology Research Center of Shandong Province, College of Chemistry and Material Science, Shandong Agricultural University, Tai'an, Shandong 271018, People's Republic of China

or incineration, thereby leading to economic waste and environmental pollution [16]. Leftover rice (LR) is a major part of kitchen waste, which is composed of abundant starch and a small amount of protein and lipid [17]. They are all common biomass resources. Zhou et al. used LR for controlled-release urea fertilizer hydrogels [18]. Zou et al. prepared hierarchical porous carbons with high specific surface area and large mesoporosity by LR [19]. To the best of our knowledge, there is no report on using LR for food packaging, and thus, we took advantage of LR by interpenetrating network technology to develop the IPN food packaging films with enhanced properties. Gelatin (GEL) is an animal origin protein obtained by hydrolysis of collagen, which presents in skin and cartilage of pigs output, bovine hides, bones, and other sources [20]. It has a good film-forming, high mechanical, oxygen barrier, and translucency properties [21,22]. Marvizadeh et al. used tapioca starch, GEL, and nanorod ZnO to prepare bionanocomposite film in food and pharmaceutical packaging [23]. Glycerol with polyhydroxy groups as a plasticizer affected the structure and performance of the materials [24].

The objective of this work is to fabricate innovative IPN films for food packaging. The IPN films were synthesized using LR and GEL by interpenetrating network technology. The formation of the IPN structure not only increases the dense structure of films but also improves the properties of films. The structure and properties of the IPN films were determined to provide the guides for the future development of eco-friendly food packaging.

2 Materials and methods

2.1 Materials

GEL extracted from cowhide was provided by Oceanwide Biotechnology Co., Ltd. (Guangdong, China). The LR came from the canteen of Shandong Agricultural University (Shandong, China). The raw materials were dried at 60°C for 12 h and then crushed for 30 min with a pulverizer (Changhong Pharmaceutical Machinery Factory Co., Ltd, Changsha, China) at room temperature. The obtained LR powder was passed through 300 mesh sieves. Glycerol was purchased from Sinopharm Chemical Reagent Co., Ltd. (Shanghai, China).

2.2 Preparation of films

All films from LR and GEL were prepared according to previous literature with some changes [25]. LR was heated in a water bath at 70°C for 30 min. GEL was dissolved in a water bath at 45°C until a clear solution was obtained. After dissolution, LR and GEL solution was mixed through ultrasonication (Kunshan Ultrasonic Instrument Co., Ltd, Kunshan, China) 15 min at 45°C. Glycerol, as a plasticizer (35% of the LR mass), was added into the above mixture solution in a 45°C water bath and continued stirring for 30 min. Then, the mixture was poured onto 20 × 20 cm plexiglass plates. Finally, the films were dried for 24 h at room temperature. The resultant films were placed in a constant temperature and humidity box of 53% RH and 23°C for 48 h before characterization. All films were obtained at different mass ratios of LR/GEL (100/0, 100/10, 100/20, 100/30, 100/40, 100/50, w/w), and the corresponding films were labeled as LR, IPN10, IPN20, IPN30, IPN40, and IPN50, respectively. The preparation process of LR and IPN films is proposed in Scheme 1.

2.3 Characterization

2.3.1 Fourier transform infrared (FTIR) spectroscopy

The FTIR spectra of GEL powder, LR, and IPN films were analyzed by a TENSOR II FTIR spectrometer (Bruker,

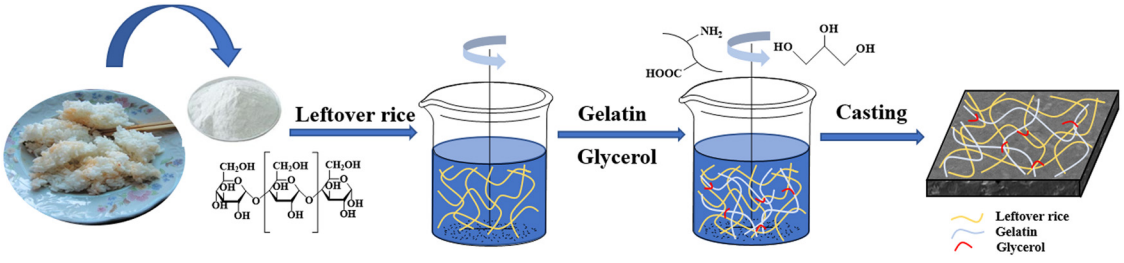

Scheme 1: Diagram of the fabrication process of LR and IPN films.

Germany) with a Smart iTR diamond ATR accessory using a resolution of 4 cm^{-1} over a wavenumber range from 4,000 to 400 cm^{-1}.

2.3.2 X-ray diffraction (XRD)

The XRD patterns of the GEL powder, LR, and IPN films were obtained by an X-ray diffractometer (Smartlab, Rigaku, Japan) which is equipped with a copper source. The samples were scanned in the angular range of 2θ = 5–35° with the scanning rate of 0.02°/s.

2.3.3 Scanning electron microscopy (SEM)

The surface with the plexiglass plate side and cross-section morphology of the films were observed using JSM-6610LV SEM (JEOL, Japan). These images were taken at a magnification of 1,000 times with a 15 kV potential. The cross-section of samples was prepared by cooling the films in liquid nitrogen and then cracking them. All films were adhered to the aluminum base with conductive adhesive tape and sprayed with gold on an IB-V ion sputtering instrument.

2.3.4 Atomic force microscopy (AFM)

AFM images of films with the plexiglass plate side were obtained using a Multimode Nanoscope IIIa controller (Veeco, USA). The plane and three-dimensional images of films were observed. Average roughness and root-mean-square roughness statistical parameters were calculated to analyze the roughness of the films. The tapping mode was used during measurement.

2.3.5 Thermogravimetric analysis (TGA)

The thermal properties of films were characterized using DTG-60A thermogravimetric analyzer (SHIMADZU, Japan). The films with a mass of about 5–10 mg placed in an alumina crucible were heated from room temperature to 600°C at a heating rate of 10°C/min. The nitrogen flow rate as the purge gas was 50 mL/min [21].

2.3.6 Water contact angle

The water contact angles were measured by the contact angle instrument (JC2000D1, Zhongchen Digital Technology Apparatus Co., Ltd, Shanghai, China) to estimate the surface hydrophobicity of the films [26]. The films (50 × 10 mm) were placed on a horizontally movable platform before the measurement. Five microliter water droplet was dropped on the smooth surface of the films and measured. At least five parallel measurements were taken in different positions on the surface of each sample to provide an average value.

2.3.7 Moisture content

The moisture content of the films was measured according to the method of previous reports with slight modification [27,28]. The films balanced at 23°C and 53% humidity were cut into a square of 20 × 20 mm, and the initial mass $M1$ was recorded. Next, the films dried at 105°C for 24 h were recorded as $M2$. Finally, the moisture content of films was obtained according to the following equation:

$$\text{Moisture content } (\%) = [(M1 - M2)/M1] \times 100\%. \quad (1)$$

2.3.8 Visible light transmittance and haze

The optical properties of the films were measured using a light transmittance/haze meter (WGT-2S Shenguang Co., Ltd, Shanghai, China) according to the industry standard of the GB/T 2410-2008. The films were cut into a 50 × 50 mm square placed between the magnetic clamps, selecting C light source (6,774 K). Each film was measured at five different positions and the average value was taken for the thickness of the film.

2.3.9 Water vapor permeability (WVP)

WVP was measured by W3-031 Water vapor transmittance tester (Labthink Instruments Co., Ltd, Jinan, China). The characterization was conducted according to the method of previous reports with slight modification [29]. The films were cut into a circle with an area of 33.18 cm^2 and placed in the perspective cup. Then, the films were preheated for 4 h at 38°C and 90% relative humidity and measured. At least five parallel measurements were taken on each sample to provide an average value.

2.3.10 Oil absorption measurement

The 2 × 2 cm films were weighed (M_b) and placed in 20 mL peanut oil at room temperature. After 4 h, the films were

taken out and the surface oil was wiped off with filter paper to obtain the final weight (M_a) [30]. The oil absorption of films was calculated according to the following equation:

$$\text{Oil absorption } (\%) = [(M_a - M_b)/M_b] \times 100\%. \quad (2)$$

2.3.11 Mechanical properties

The films with temperature and humidity balance were cut into a rectangle of 150 × 15 mm. According to ASTM D882-18 (ASTM, 2018), the tensile strength (TS, MPa), elongation at break (EAB, %), and Young's modulus (YM, MPa) of the films were measured by XLW automatic tensile tester (Labthink Instruments Co. Ltd). The initial distance of the fixture was 100 mm, and the tensile speed was 100 mm/min. At least five parallel measurements were taken on each sample to provide an average value [29].

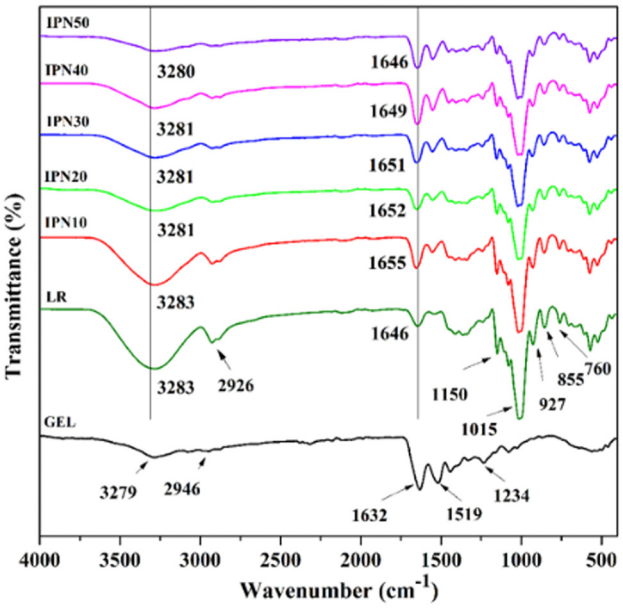

Figure 1: FTIR spectroscopy of GEL powder, LR, and IPN films.

2.4 Statistical analysis

Analysis of variance of experimental data was obtained by SPSS Statistics 21 software (IBM Co., New York, NY, USA). Duncan's multiple range test was used for differential analysis of multiple sets of samples with confidence level as $p < 0.05$.

3 Results and discussion

3.1 FTIR analysis

The FTIR spectra of GEL powder, LR, and IPN films are shown in Figure 1. For the GEL, the extremely broad peak at 3,279 cm^{-1} was the –OH and N–H groups stretching vibrations corresponding to the Amide-A band of GEL. The Amide-B band representing the asymmetric stretching vibration of =C–H and $-NH_3^+$ appeared at 2,946 cm^{-1}. Amide-I band located around 1,632 cm^{-1} represented C=O stretching vibration, which coupled with CN stretching, CCN deformation, and in-plane NH bending modes [31]. It is the most sensitive spectral region of protein secondary structure. The Amide-II band of GEL was found at 1,519 cm^{-1}, which was related to the stretching vibrations of C–N groups and the bending vibration of N–H groups in GEL molecules. The Amide-III region was noticeable at the wavenumbers of 1,234 cm^{-1}, which represents the combination peaks between C–N stretching vibrations and N–H deformation of the amide bond, as well as absorptions arising from wagging vibrations of the CH_2 groups from the GEL. The FTIR spectrum of LR film shows some obvious absorption peaks at 3,283, 2,926, and 1,646 cm^{-1} ascribed to O–H stretching vibration, C–H stretching vibration, and water molecules absorbed in the amorphous regions in starch, respectively. The weak peaks at 1,150 cm^{-1} ascribed to C–O stretching vibration of C–OH and 1,015 cm^{-1} corresponded to the stretching vibration of C–O–C occurred in the FTIR spectrum of LR film [32]. The signal of 855 cm^{-1} was attributed to the deformation of CH_2, indicating the α-configuration of starch. Typical peaks of starch occurred at 927 and 760 cm^{-1}, which indicated α-1, 6-D-glucosidic linkage, and α-1, 4-D-glucosidic linkage of starch, respectively.

Moreover, it can be seen from the FTIR spectrum that the hydroxyl peaks of the IPN films were shifted to the lower values than that of LR film. This indicated the amino groups and hydroxyl groups on the GEL chains reacted with hydroxyl groups of LR. Besides, it was found that the intensity of peaks of hydroxyl groups in the IPN films gradually decreased with the increase in GEL content, and this showed an incremental reaction between LR and GEL, thereby resulting in the decrease in reactive hydroxyl groups content. Moreno et al. also found that starch-GEL film exhibited lower strength in different bands, especially those associated with the vibration of hydroxyl groups. They pointed out that this may relate to the strong interaction between the two polymers chains to form new

bonds and a denser network structure [33]. Therefore, the FTIR spectra showed that the GEL chains not only physically blended with LR chains but also chemically reacted with LR in the IPN films systems.

3.2 XRD analysis

XRD is a powerful technique for analyzing the crystal structure of polymers [34]. The XRD pattern of the LR and IPN films possessed an amorphous large broad peak at 2θ = 15.3–30.8° shown in Figure 2. The broad peak of LR film at 2θ = 19.8° represented B-type crystalline structure starch. The IPN films showed two diffraction peaks around the peaks at 2θ = 7.6° and 2θ = 22.3° corresponded to the triple-helical crystalline structure of denatured collagen in GEL [35,36]. Furthermore, the intensity of peaks was suppressed when the GEL content increased in the IPN films, indicating the incorporated GEL disrupted the ordered structures of the polymeric matrix of LR. That is, the increase in GEL content resulted in a decreased crystallinity of LR in IPN films, which was favorable to the flexibility of films and the formation of interpenetrating network structure.

3.3 SEM and AFM analysis

SEM can be used to directly observe the microstructure morphology of the LR and IPN films. Figure 3 shows the surface and cross-section of LR and IPN films. It was observed from SEM in Figure 3a1 that some irregular white particles were accumulated on the surface, forming a rough surface. These IPN films generally showed smoother surfaces than LR film. The well-distributed matrix was observed in the IPN30 and IPN40 films with smoother surfaces and fewer protrusions. The smoothness of film surface may be that the incorporation of GEL enhances the intermolecular and intramolecular hydrogen bonds, thereby increasing the TS of the films. However, some bumps accumulated on the surface of IPN50 film, probably because of too much GEL contents in the film. These resulted in the poor compatibility among components in IPN50 film, which affected the formation of interpenetrating network structure to a great extent. Therefore, the mechanical properties have not changed much. To further investigate the surface morphology of the films, AFM measurements were performed on the LR and IPN30 film. Figure 3 shows the AFM image (3D and plane) of the LR and IPN30 films. The LR film presents a rough surface with R_a value (119 nm) and R_q value (149 nm) compared with the IPN30 film (R_a: 33.0 nm, R_q: 46.9 nm). From the phenomenon of SEM and AFM, the IPN30 and IPN40 films had been proven to allow good compatibility on the molecular scale and well-distributed dispersion, thus forming a smoother surface.

Furthermore, many fibrous-oriented wrinkles were randomly distributed on the cross-section of the LR, IPN10, IPN20, and IPN30 films. This phenomenon may be caused by a large amount of amylose present in the starch system. Gutierrez et al. also found a similar morphology in the films from yam and tapioca starch [37]. It was noted that the brittle phenomenon was observed in the IPN40 and IPN50 films, especially in the IPN50 films. It was related to the reduction of the plasticizer in the system of IPN films, which resulted to decrease in EAB. Because of the ordered structure formed between LR and GEL chains without inappropriate layering, the moderate GEL content (IPN40) increased the smoothness of the film surface, but it was counter-productive to be excessive GEL content. The compactness of the interpenetrating network and dispersion of LR and GEL in the film systems resulted in different structures and properties such as thermal properties, water vapor barrier properties, and mechanical properties.

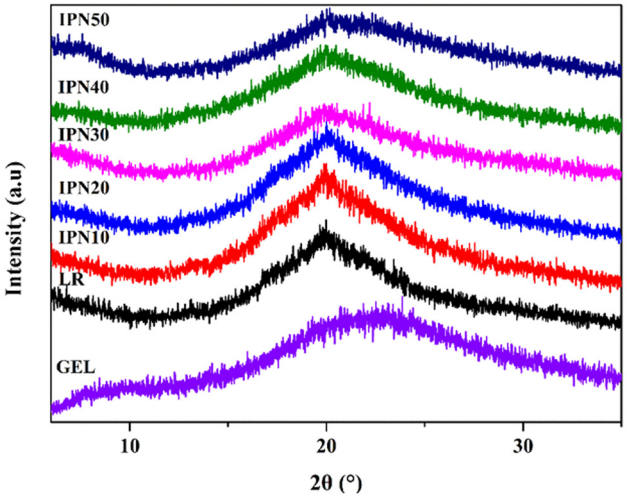

Figure 2: XRD patterns of GEL powder, LR and IPN films.

3.4 Thermal properties

To study the thermal properties of the LR and IPN films, TGA was performed (Figure 4). Three main thermal degradation stages were observed in the TGA curves of

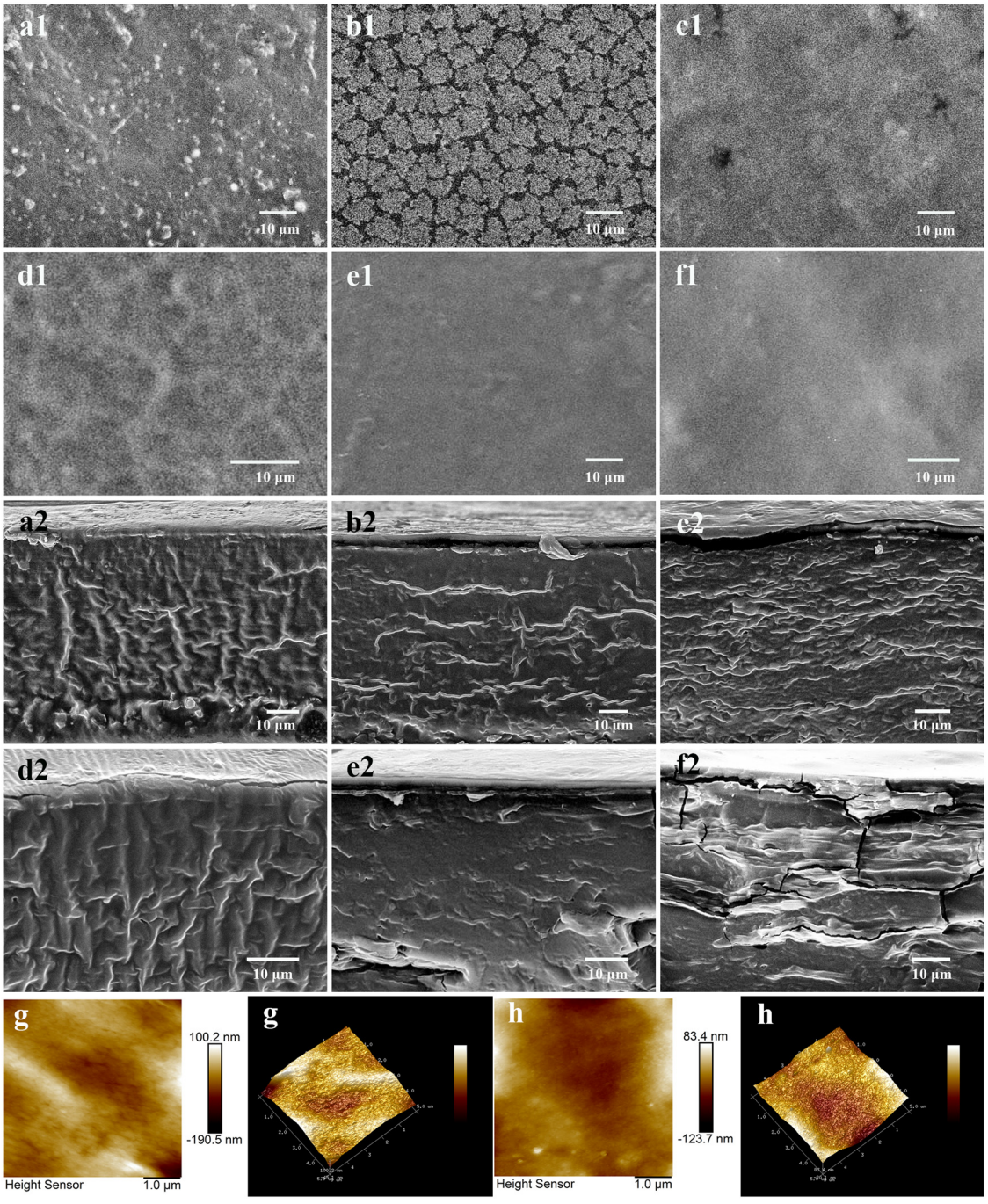

Figure 3: SEM and AFM images of LR and IPN films: surface of LR (a1), IPN10 (b1), IPN20 (c1), IPN30 (d1), IPN40 (e1), and IPN50 (f1) films at 1,000× magnification; cross-section of LR (a2), IPN10 (b2), IPN20 (c2), IPN30 (d2), IPN40 (e2), and IPN50 (f2) films at 1,000× magnification. AFM image (plane and 3D) of LR (g) and IPN30 (h) films.

the IPN and LR films. The first one (50–150°C) was observed because of the evaporation of free water and bound water in the films. The second one was from 150°C to 350°C, which was associated with the decomposition of glycerol, polysaccharides, and low molecular weight proteins. The third section (350–600°C) was due to the decomposition of easily degradable amino acid fragments, depolymerization of protein helix structure.

The main thermal properties for the LR and IPN films with different LR/GEL ratios are listed in Table 1. At the initial stage, the 5% weight loss temperature ($T_{5\%}$) of IPN30, IPN40, and IPN50 films had higher values

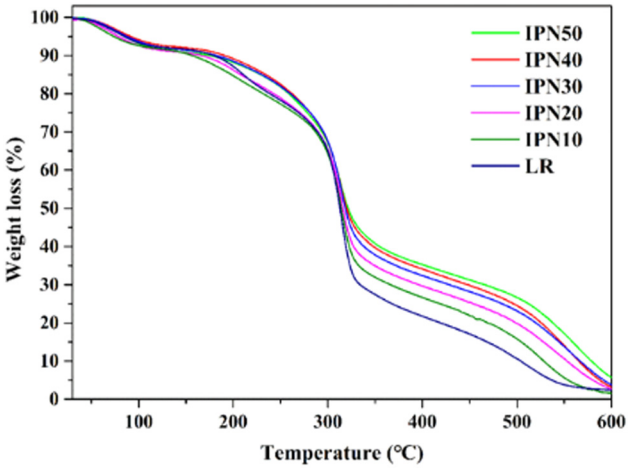

Figure 4: TGA curves of LR and IPN films.

compared with that of LR film, whereas $T_{5\%}$ of IPN10 and IPN20 films had lower values compared with that of LR film. It may be related to the decomposition of uncrosslinked oligomer in IPN10 and IPN20 network systems. With the increase in decomposition temperature, the LR and GEL in the IPN films gradually decomposed. It was observed that the $T_{50\%}$ and $T_{80\%}$ of the IPN films shifted toward higher values than those of LR film, suggesting that the IPN films had higher thermal resistance than the LR film, because the stronger interaction between the LR and GEL chains led to the formation of the denser network structure in the IPN films, thereby increasing the thermal property of IPN films. Silva et al. also found that starch/GEL films had higher thermal stability than starch, resulting from the strong interaction between the components of the films [38]. Increasing GEL concentration led to better enhancement in the structural integrity within the IPN films matrix. However, adding too much GEL network affected the formation of IPN structure, thereby causing the poor dispersion in the film systems. Therefore, when the GEL contents in IPN films were more than 30%, the thermal properties of IPN films were not different, that is, the thermal properties of IPN30, IPN40, and IPN50 films were a little similar. The strong hydrogen bonds between LR and GEL improved the compatibility of polymer chains, thereby promoting the formation of interpenetrating network structure, as well as optimizing the thermal stability of the IPN films.

Table 1: Summary of thermal properties of IPN and LR films

Samples	$T_{5\%}$ (°C)	$T_{50\%}$ (°C)	$T_{80\%}$ (°C)
LR	84.68	312.81	419.28
IPN10	73.64	314.16	469.16
IPN20	78.23	315.84	498.93
IPN30	87.36	318.49	520.19
IPN40	91.47	319.84	525.80
IPN50	85.14	321.43	538.03

3.5 Water contact angle of films

The static water contact angle measurements can be used to investigate the wettability properties of all films. The images of the LR and IPN films are shown in Figure 5. It was observed that the water contact angle of the LR film was only 47.6°. For the IPN10, IPN20, IPN30, IPN40, and IPN50 films, water contact angles were 85.7°, 92.0°, 107.8°, 113.4°, and 117.5°, showing a hydrophobic character, respectively. The IPN films were obviously increased by 80.0–146.8%, which indicated higher hydrophobicity of the IPN films compared with that of the LR film. It indicated that the addition of the GEL network pronouncedly improved the water resistance of IPN films. This result may be because of the decrease in hydrophilic groups on the surface of the IPN films in which the hydroxyl groups on the LR chains reacted with amino groups and hydroxyl groups on the GEL chains, thereby raising the water resistance of IPN films, compared with that of LR film.

Moreover, it was interestingly noted from Figure 5 that the hydrophobicity of the IPN films increased with increasing GEL content, but the GEL contents in IPN films were more than 30%; the water contact angle of IPN films had an insignificant increase. The result may be correlated with the too much GEL chains existed in the IPN films. When the GEL contents in IPN films were higher in the IPN films (50%), the more GEL chains were difficult to react with LR network and aggregated on the surface of films (as shown in Figure 3), thus exposing more hydrophilic functional groups on the surface of IPN50 films and consequently causing no significant increase in the contact angle compared with IPN40 films. Combined with moisture content characterization, the water contact angle increased while the moisture content decreased, which agreed with the relationship between moisture content and water contact angle reported by Leceta et al. [39]. This was also consistent with the conclusion that the hydrophobicity of the IPN films was improved. Therefore, the incorporation of the GEL network has a significant effect on the formation of IPN, thereby improving the water contact angle of the IPN films.

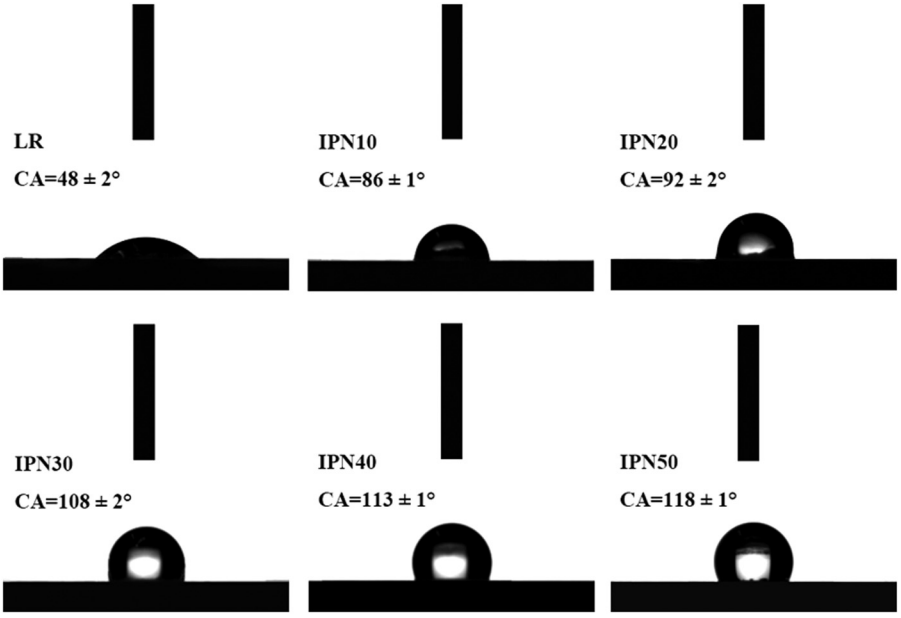

Figure 5: Water contact angle measurement of LR and IPN films.

3.6 Optical properties of film

The light intensity through the films can affect how well people see the object inside the packaging. As shown in Figure 6a, the addition of GEL increased the transmittance of the IPN films from 73.75% to 84.44% and reduced the haze of the IPN films from 86.33% to 66.10%, which meant that the gloss and transparency of the IPN films were improved, especially the degree of imageability. The SEM showed an uneven surface of LR film, which may be responsible for its low transmittance. Therefore, the formation of interpenetrating network structure between LR and GEL was the important factor in reducing light scattering and allowed the easy passage of light. Besides, the addition of GEL into the polymer matrix may result in a more open structure of the triple helix, making the light more permeable in the films. In contrast, the semi-crystalline starch in the LR film acts as a barrier of light to scatter some of the light, resulting in a decrease in the transmittance of the LR film. Because of the presence of glycosides rings from the starch, high concentration of starch may enable a less opened matrix, which may hinder the passage of light [40].

Furthermore, with the increase in GEL content, the transmittance of the IPN films was increased and the haze of the IPN films was decreased. These results can be explained by the compact mutual entanglement and network crosslinking of LR and GEL chains. However, it was a little change in the transmittance of the IPN30 (81.02%), IPN40 (82.37%), and IPN50 (84.44%) films. It was probably because excessive GEL contents cannot participate in the formation of IPN structure, thereby further hindering the passage of more light. Besides, the IPN40 (66.10%) and IPN50 (66.38%) films showed no significant change in the haze, indicating that the transmittance and the haze of IPN films did not always have an inverse relationship. It can be because the factors such as the film production process, the additives used, and the surface state had different effects on the transmittance and the haze of films. Combined with XRD characterization, the decrease in crystallinity also improved the optical properties of the films. The findings obtained in this study were in agreement with the result reported by Fakhouri et al. who studied the addition of GEL increased the opacity of corn starch biofilms [40]. In general, the excellent optical properties of the films can be attributed to the use of GEL to make good interactions between molecules in the IPN system.

3.7 Water vapor barrier properties of film

The water vapor barrier properties of films are an important indicator of food packaging applications, which directly affects shelf life and food-nutrient loss. The WVP is to investigate the transfer of water between food and the surrounding environment. To study the effects of the interpenetrating network structure on the water vapor barrier properties of IPN films in this work, the WVP of the LR and IPN films was measured. As shown in Figure 6b, the WVP of the IPN films ranged from 1.26×10^{-12} to 1.03×10^{-12} (g cm/(cm^2 s Pa)) and

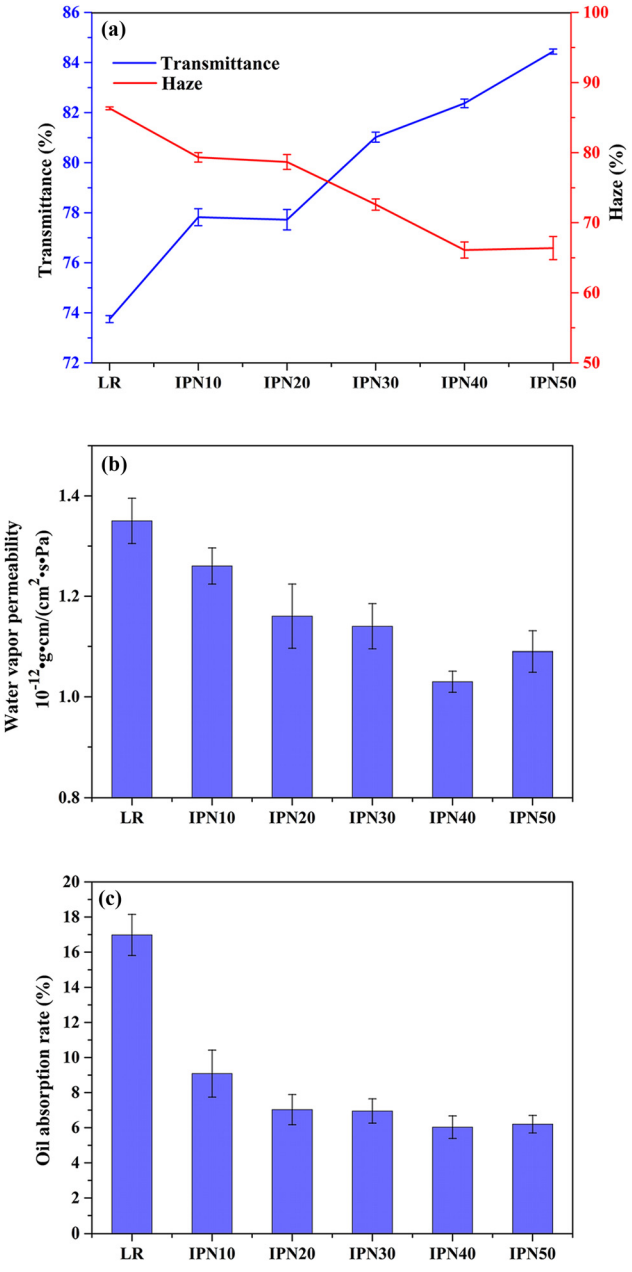

Figure 6: Visible light transmittance and haze (a), WVP (b), and oil absorption (c) of LR and IPN films.

the WVP of the LR film was 1.35×10^{-12} (g cm/(cm^2 s Pa)), significantly indicating the excellent water vapor barrier properties of IPN films. It also showed that the IPN films had a lower free volume availability and the more compact structure. The result suggested that the formation of the interpenetrating network structure of the IPN films effectively reduced the penetration of water vapor into the packaging. At the same time, we found that the WVP of the IPN films gradually decreases as the GEL content increases (Figure 6b). Soo et al. thought the hydrophobic amino acids in the GEL system caused the lowest WVP value showed in GEL/rice flour films [25]. Moreover, the moisture content of the LR film was very high (shown in Table 2); the high moisture content can cause the swelling of films, which affected the conformational change of the film's microstructure. The swollen films not only increased the moisture absorption but also caused the formation of some channels in the polymer film, thereby resulting in the increased permeate flow. Therefore, the IPN films, especially the IPN40 film, were advantageous for improving the water vapor barrier properties of the films.

3.8 Oil absorption properties

To prevent the oil oozing out when wrapping oily articles or articles containing liquid oil, the food packaging needs to have a certain oil resistivity property. It can be seen in Figure 6c that the oil resistivity properties of all films were different. The LR film had the highest oil absorption rate (16.98%). For the IPN10, IPN20, IPN30, IPN40, and IPN50 films, oil absorption rates were 9.08%, 7.03%, 6.95%, 6.03%, and 6.20%, respectively. The oil absorption rates of IPN films decreased by 87–182% compared with that of LR film, exhibiting excellent oil resistivity property. It suggested that the incorporation of the GEL had an outstanding effect on the formation of the IPN

Table 2: Moisture, TS, EAB, and YM of LR and IPN films

Samples	Moisture (%)	TS (MPa)	EAB (%)	YM (MPa)
LR	16.01 ± 0.56^{a}	2.42 ± 0.41^{d}	21.75 ± 3.09^{b}	101.45 ± 12.43^{d}
IPN10	15.05 ± 0.54^{b}	4.14 ± 0.41^{c}	18.63 ± 2.99^{b}	192.00 ± 12.29^{c}
IPN20	12.31 ± 0.43^{c}	4.22 ± 0.50^{c}	17.33 ± 1.01^{b}	201.67 ± 30.51^{c}
IPN30	9.56 ± 0.21^{d}	8.82 ± 0.41^{b}	9.25 ± 0.59^{c}	466.24 ± 38.13^{b}
IPN40	7.80 ± 0.82^{e}	9.37 ± 0.46^{b}	3.78 ± 0.36^{c}	442.58 ± 53.22^{b}
IPN50	8.23 ± 0.41^{e}	11.40 ± 0.58^{a}	3.95 ± 0.78^{c}	531.18 ± 34.42^{a}

Means followed by different lowercase letters in the same column were significantly different by Duncan's test ($P < 0.05$).

structure, thereby resulting in the excellent oil resistivity properties of IPN films. Furthermore, the oil absorption rate of the IPN films decreased with the increase in GEL content, because the dense structure reduced the dissolution of the molecule and its diffusion rate in the film. Among them, IPN40 is the lowest oil absorption rate. When the GEL content in the IPN films was more than 30%, the IPN films had a similar oil absorption rate which was consistent with the analysis of water contact angle, moisture content, and thermal and mechanical properties.

3.9 Moisture content analysis

The moisture content of the films influences the humidity atmosphere inside the packaging, thus affecting the shelf life of the food in the packaging. It can be seen from Table 2 that the moisture content of IPN films was lower, which decreased by 6.4–105% compared with that of LR film. It showed that the reaction between the amino groups and the hydroxyl groups of GEL and the hydroxyl groups of LR resulted in the formation of a denser structure in the IPN films, thereby allowing the reduction of available functional groups for water-binding molecules. Moreover, it was interestingly noted that the moisture content of IPN films decreased with increasing GEL content, and there was a similar moisture content in the IPN30, IPN40, and IPN50 systems. Among them, the IPN40 has the lowest moisture content. The result was consistent with other properties, indicating that the IPN system with more than 30% GEL content had a similar property.

3.10 Mechanical properties

Mechanical properties were measured primarily to observe the strength and toughness of the films [41]. The TS, EAB, and YM of all films are listed in Table 2. The TS and YM of the IPN films were increased about 4.7 times and 5.2 times, but EAB of the IPN films was decreased about 5.8 times compared with that of LR film, respectively. This phenomenon was largely related to a strong interaction between LR and GEL chains, thereby resulting in a decrease in the flexibility of IPN films. With the increment of GEL content, the TS and YM of the IPN films were gradually increased, whereas the EAB of the IPN films was gradually decreased. Similar results were obtained by Acosta et al. who thought that the conformation and arrangement of protein chains in the matrix resulted in strong interchain forces close to the collagen structure, thereby enhancing its mechanical properties [42]. Cao et al. also reported that the mechanical properties of the composite films were gradually increased with increasing GEL contents because triple helix interacted with soy protein to form a more organized network [43]. Therefore, the higher GEL content and better interaction of LR and GEL chains improved the TS and YM of the IPN films. This was affected by the degree of the interpenetrating network between LR and GEL chains. Moreover, the plasticizer was also an important factor affecting the mechanical properties of the IPN films. The introduction of small-molecule plasticizers into the macromolecular chain reduces intermolecular forces and enhances flexibility. The decrease in EAB of films was because of the reduction in glycerol content as a plasticizer in the IPN system, thereby resulting in the decreased flexibility of IPN films, especially more obviously in the IPN30 and IPN40 films. It was also noted from Table 2 that the moisture content and elongation at the break of IPN films with the GEL content had the same tendency. The water was also a plasticizer for these films, and the reduction of water content led to a reduction in the EAB of IPN films. Therefore, the selection of GEL content needs to be combined with the conditions of use, and the appropriate balance between TS and EAB.

4 Conclusions

In this work, the IPN films were successfully fabricated by the different ratios of LR and GEL. The FTIR spectra of the movement of amino groups and hydroxyl groups showed the intermolecular interactions between LR and GEL chains. Compared with LR film, the IPN films showed a higher density structure, better thermal stability, higher water contact angle, lower oil absorption rate, and better moisture barrier properties, especially the IPN40 film. Furthermore, the introduction of GEL contents in IPN films increased crosslinking degree, thereby improving TS and YM of IPN films. These characterizations showed that the incorporation of GEL in the IPN films can effectively improve the performance of the films. The LR is still viable as cost-effective sources to recycle and has outstanding potential for the sustainable development of the application in food packaging while reducing kitchen waste.

Research funding: This research was funded by National Key R & D Program of China, grant number: 2017YFD0200706.

Author contributions: Sijia Li: Writing – original draft, conceptualization, methodology, validation, and investigation; Chun Shao: Methodology and formal analysis; Zhikun Miao: Data curation and supervision. Panfang Lu: Writing – review and editing, conceptualization, supervision, funding acquisition, and project administration.

Conflict of interest: The authors state no conflict of interest.

References

[1] Vudjung C, Chaisuwan U, Pangan U, Chaipugdee N, Boonyod S, Santawitee O, et al. Effect of natural rubber contents on biodegradation and water absorption of interpenetrating polymer network (IPN) hydrogel from natural rubber and cassava starch. Energy Procedia. 2014;56:255–63.

[2] Niu Y, Xia Q, Gu MD, Yu LL. Interpenetrating network gels composed of gelatin and soluble dietary fibers from tomato peels. Food Hydrocolloid. 2019;89:95–9.

[3] Hu MJ, Wu ZY, Sun L, Guo SY, Li HB, Liao J, et al. Improving pervaporation performance of PDMS membranes by interpenetrating polymer network for recovery of bio-butanol. Sep Purif Technol. 2019;228:115690–700.

[4] Kamboj S, Singh K, Tiwary AK, Rana V. Optimization of microwave assisted Maillard reaction to fabricate and evaluate corn fiber gum-chitosan IPN films. Food Hydrocolloid. 2015;44:260–76.

[5] Jindal M, Kumar V, Rana V, Tiwary AK. Physico-chemical, mechanical and electrical performance of bael fruit gum–chitosan IPN films. Food Hydrocolloid. 2013;30:192–9.

[6] Li X, Zheng Y, Pan Q, Li CY. Polymerized ionic liquid-containing interpenetrating network solid polymer electrolytes for all-solid-state lithium metal batteries. ACS Appl Mater Inter. 2019;11:34904–12.

[7] Gu P, Li B, Wu BS, Wang JP, Müller-Buschbaum P, Zhong Q. Controlled hydration, transition, and drug release realized by adjusting layer thickness in alginate-Ca^{2+}/poly (N-isopropylacrylamide) interpenetrating polymeric network hydrogels on cotton fabrics. ACS Biomater Sci Eng. 2020;6:5051–60.

[8] Zhang CM, Chen YJ, Li H, Liu HZ. Facile fabrication of polyurethane/epoxy IPNs filled graphene aerogel with improved damping, thermal and mechanical properties. RSC Adv. 2018;8:27390–9.

[9] Swain S, Bal T. Microwave irradiated Carrageenan-Guar gum micro-porous IPN: a novel material for isotropic tissue scaffolding. Int J Polym Mater Polym Biomater. 2019;68:796–804.

[10] Tabari M. Investigation of carboxymethyl cellulose (CMC) on mechanical properties of cold water fish gelatin biodegradable edible films. Food. 2017;6:41–8.

[11] Li JY, Liu HH, Paul Chen J. Microplastics in freshwater systems: a review on occurrence, environmental effects, and methods for microplastics detection. Water Res. 2018;137:362–74.

[12] Mao A, Xu WT, Xi EH, Li Q, Wan H. Evaluation of phenol-formaldehyde resins modified and blended with pyrolysis bio-oil for plywood. For Pro J. 2018;68:113–9.

[13] Nair SS, Zhu JY, Deng YL, Ragauskas AJ. High performance green barriers based on nanocellulose. Sustain Chem Pro. 2014;2:23–30.

[14] Parisa P, Luke PB, Rina T, Hamid G. Biomimetic synthesis of two different types of renewable cellulosic nanomaterials for scaffolding in tissue engineering. Green Process Synth. 2018;7:181–90.

[15] Sakaguchi L, Pak N, Potts MD. Tackling the issue of food waste in restaurants: options for measurement method, reduction and behavioral change. J Clean Prod. 2018;180:430–6.

[16] Tsang YF, Kumar V, Samadar P, Yang Y, Lee J, Ok YS, et al. Production of bioplastic through food waste valorization. Env Int. 2019;127:625–44.

[17] Jia C, Lu PF, Zhang M. Preparation and characterization of environmentally friendly controlled release fertilizers coated by leftovers-based polymer. Processes. 2020;8:417–32.

[18] Zhou T, Wang Y, Huang S, Zhao YC. Synthesis composite hydrogels from inorganic-organic hybrids based on leftover rice for environment-friendly controlled-release urea fertilizers. Sci Total Env. 2018;615:422–30.

[19] Zou ZM, Jiang CH. Hierarchical porous carbons derived from leftover rice for high performance supercapacitors. J Alloy Compd. 2020;815:152280–7.

[20] Abedinia A, Mohammadi Nafchi A, Sharifi M, Ghalambor P, Oladzadabbasabadi N, Ariffin F, et al. Poultry gelatin: characteristics, developments, challenges, and future outlooks as a sustainable alternative for mammalian gelatin. Trends Food Sci Tech. 2020;104:14–26.

[21] Wang K, Wang WH, Ye R, Xiao JD, Liu YW, Ding JS, et al. Mechanical and barrier properties of maize starch–gelatin composite films: effects of amylose content. J Sci Food Agr. 2017;97:3613–22.

[22] Limpisophon K, Schleining G. Use of gallic acid to enhance the antioxidant and mechanical properties of active fish gelatin film. J Food Sci. 2017;82:80–9.

[23] Marvizadeh MM, Oladzadabbasabadi N, Mohammadi Nafchi A, Jokar M. Preparation and characterization of bionanocomposite film based on tapioca starch/bovine gelatin/nanorod zinc oxide. Int J Biol Macromol. 2017;99:1–7.

[24] Li Q, Li M, Chen C, Cao GM, Mao A, Wan H. Adhesives from polymeric methylene diphenyl diisocyanate resin and recycled polyols for plywood. For Prod J. 2017;67:275–82.

[25] Soo PY, Sarbon NM. Preparation and characterization of edible chicken skin gelatin film incorporated with rice flour. Food Packaging Shelf. 2018;15:1–8.

[26] Merino D, Gutiérrez TJ, Mansilla AY, Casalongué CA, Alvarez VA. Critical evaluation of starch-based antibacterial nanocomposites as agricultural mulch films: study on their interactions with water and light. ACS Sustain Chem Eng. 2018;6:15662–72.

[27] Priyadarshi R, Sauraj Kumar B, Deeba F, Kulshreshtha A, Negi YS. Chitosan films incorporated with Apricot (Prunus armeniaca) kernel essential oil as active food packaging material. Food Hydrocolloid. 2018;85:158–66.

[28] Tsai M-J, Weng Y-M. Novel edible composite films fabricated with whey protein isolate and zein: preparation and physicochemical property evaluation. LWT. 2019;101:567–74.

[29] Zhang R, Wang WT, Zhang H, Dai YY, Dong HZ, Hou HX. Effects of hydrophobic agents on the physicochemical properties of edible agar/maltodextrin films. Food Hydrocolloid. 2019;88:283–90.
[30] Li M, Zhao ZL, Zhou X, Fan L. Optimization of disposable tableware based on soybean dregs by response surface method (in Chinese). Process Agric prod. 2019;475:1–5.
[31] Nazmi NN, Isa MIN, Sarbon NM. Preparation and characterization of chicken skin gelatin/CMC composite film as compared to bovine gelatin film. Food Biosci. 2017;19:149–55.
[32] Seligra PG, Medina Jaramillo C, Famá L, Goyanes S. Biodegradable and non-retrogradable eco-films based on starch–glycerol with citric acid as crosslinking agent. Carbohydr Polym. 2016;138:66–74.
[33] Moreno O, Cárdenas J, Atarés L, Chiralt A. Influence of starch oxidation on the functionality of starch-gelatin based active films. Carbohydr Polym. 2017;178:147–58.
[34] Zhang X, Liu YL, Lu PF, Zhang M. Preparation and properties of hydrogel based on sawdust cellulose for environmentally friendly slow release fertilizers. Green Process Synth. 2020;9:139–52.
[35] Peña C, de la Caba K, Eceiza A, Ruseckaite R, Mondragon I. Enhancing water repellence and mechanical properties of gelatin films by tannin addition. Bioresour Technol. 2010;101:6836–42.
[36] Liu J, Yong HM, Liu YP, Qin Y, Kan J, Liu J. Preparation and characterization of active and intelligent films based on fish gelatin and haskap berries (*Lonicera caerulea* L.) extract. Food Packaging Shelf. 2019;22:100417–27.
[37] Gutiérrez TJ, Tapia MS, Pérez E, Famá L. Structural and mechanical properties of edible films made from native and modified cush-cush yam and cassava starch. Food Hydrocolloid. 2015;45:211–7.
[38] Chaves da Silva NM, Fakhouri FM, Fialho RLL, Cabral Albuquerque ECDM. Starch–recycled gelatin composite films produced by extrusion: physical and mechanical properties. J Appl Polym Sci. 2018;135:46254–63.
[39] Leceta I, Guerrero P, de la Caba K. Functional properties of chitosan-based films. Carbohydr Polym. 2013;93:339–46.
[40] Fakhouri FM, Martelli SM, Caon T, Velasco JI, Mei LHI. Edible films and coatings based on starch/gelatin: film properties and effect of coatings on quality of refrigerated red crimson grapes. Postharvest Biol Technol. 2015;109:57–64.
[41] Cazón P, Velazquez G, Ramírez JA, Vázquez M. Polysaccharide-based films and coatings for food packaging: a review. Food Hydrocolloid. 2017;68:136–48.
[42] Acosta S, Jiménez A, Cháfer M, González-Martínez C, Chiralt A. Physical properties and stability of starch-gelatin based films as affected by the addition of esters of fatty acids. Food Hydrocolloid. 2015;49:135–43.
[43] Cao N, Fu YH, He JH. Preparation and physical properties of soy protein isolate and gelatin composite films. Food Hydrocolloid. 2007;21:1153–62.